

1 **Observational evidence for a stability Iris effect**
2 **in the Tropics**

3 **Marion Saint-Lu ¹, Sandrine Bony ¹, Jean-Louis Dufresne ¹**

4 ¹Laboratoire de Météorologie Dynamique (LMD) / Institut Pierre Simon Laplace (IPSL), Sorbonne
5 Université / CNRS / École Normale Supérieure / École Polytechnique, Paris, France

6 **Key Points:**

- 7 • Spaceborne lidar observations show that anvil clouds rise and reduce their cov-
8 erage when the tropics warm
9 • Observations and meteorological reanalyses support the stability-Iris effect mech-
10 anism
11 • There is evidence for a stability Iris effect over a large range of spatial scales

Corresponding author: Marion Saint-Lu, marion.saint-lu@lmd.jussieu.fr

Abstract

Anvil clouds cover extensive areas of the tropics, and their response to global warming can affect cloud feedbacks and climate sensitivity. A growing number of models and theories suggest that, when the tropical atmosphere warms, anvil clouds rise and their coverage decreases, but observational support for this behavior remains limited. Here we use 10 years of measurements from the spaceborne CALIPSO lidar to analyze the vertical distribution of clouds and isolate the behavior of anvil clouds. On the interannual time-scale, we find a strong evidence for anvils rise and coverage decrease in response to tropical warming. Using meteorological reanalyses, we show that this is associated with an increase in static stability and with a reduction in clear-sky radiatively-driven mass convergence at the anvils height. These relationships hold over a large range of spatial scales. This is consistent with the stability Iris mechanism suggested by theory and modeling studies.

Plain Language Summary

Anvil clouds cover about 40% of the tropics. Their response to global warming, especially changes in their height or in their horizontal extent, has the potential to affect the Earth's surface temperature. By analyzing 10 years of observations of the vertical distribution of clouds from a spaceborne lidar, we show that the anvils rise and reduce their coverage during the years that are anomalously warm. By using meteorological reanalyses, we further show that this behavior is consistent with the stability Iris effect suggested by theory and modeling studies. These results improve our physical understanding of the response of tropical clouds to warming, and present relationships that may be used to test climate models.

1 Introduction

Anvil clouds cover extensive areas of the tropics, reflect solar radiation and reduce outgoing long-wave radiation. In case global warming would affect their height and coverage, this could influence climate sensitivity (Zelinka & Hartmann, 2010; Hartmann, 2016; Su et al., 2017). The Fixed Anvil Temperature (FAT) hypothesis states that anvils rise nearly isothermally when the tropics warm (Hartmann & Larson, 2002). According to FAT, anvils are formed by convective detrainment, and the altitude of maximum detrainment is constrained, through mass conservation, by the convergence of mass in the surrounding clear-sky upper troposphere. The latter is due to the vertical gradient of subsidence, which is primarily driven by the decrease with height of the radiative cooling by water vapor. The variation of water vapor with height is very much constrained by the Clausius-Clapeyron thermodynamical relationship, and therefore the temperature at which the clear-sky radiative cooling drops is relatively invariant with surface temperature. When the surface warms, it rises in step with the isotherms, and therefore the peaks of the clear-sky radiatively-driven mass convergence and of the associated convective detrainment rise. Zelinka and Hartmann (2010) refined this theory and formulated the Proportionally Higher Anvil Temperature (PHAT) hypothesis, which states that anvils do not rise strictly isothermally but slightly warm instead, due to the sharp increase of static stability with height in the upper troposphere. Several studies have provided observational support for this theory, showing the rise of high clouds during the very strong 1997-98 El Niño event (Xu et al., 2005), the invariance of high clouds temperature relative to surface temperature over a 6-months period (Xu et al., 2007; Eitzen et al., 2009), and the good correspondence between vertical profiles of cloud fraction and radiatively-driven clear-sky mass convergence over a 10-months period (Kubar et al., 2007). These observations were then confirmed on longer periods of 4 to 6 years (Zelinka & Hartmann, 2011; Li et al., 2012; Thompson et al., 2017).

61 Analyzing geostationary satellite data, Lindzen et al. (2001) suggested that anvils
62 also reduce their coverage when the tropics warms. This behavior was referred to as an
63 “Iris effect”, by analogy with the eye’s iris. These observational results have been rebut-
64 ted, primarily on methodological grounds (Hartmann & Michelsen, 2002; Del Genio &
65 Kovari, 2002). Nevertheless, whether or not an Iris effect operates in climate remains an
66 open question (Bony et al., 2015; Mauritsen & Stevens, 2015). Zelinka and Hartmann
67 (2011) observed a reduction in the tropical high clouds cover when the tropics warm, us-
68 ing various satellite data including CloudSat radar observations (Stephens et al., 2017),
69 which were only available for 4 years at that time (including one El Niño event and one
70 La Niña event). Choi et al. (2017) focused on the western tropical Pacific, and observed
71 that convective clouds “concentrate” when the sea surface temperature rises. However,
72 observing such a limited region does not allow to conclude on inherent cloud responses
73 to surface temperature changes, since cloud systems can shift in and out of the box, due
74 to dynamical effects. More recently, using various satellite observations over 13 years for
75 the longest, Su et al. (2017) and Liu et al. (2017) reported a decrease of tropical high
76 cloud fraction in response to interannual surface warming. Su et al. (2017) proposed that
77 it was linked to the tightening of the ascending branch of the Hadley circulation, although
78 the mechanism underlying the cloud fraction decrease was not investigated in details.

79 In models, tropical warming can also be associated with a reduction of anvils cov-
80 erage (Tompkins & Craig, 1999; Zelinka & Hartmann, 2010; Khairoutdinov & Emanuel,
81 2013; Bony et al., 2016; Su et al., 2017; Cronin & Wing, 2017). With the idea that the
82 reduction of anvils coverage could be linked to their elevation and to PHAT, Bony et al.
83 (2016) proposed a thermodynamic “stability Iris” hypothesis. As the tropics warm, the
84 anvils rise and find themselves in a more stable atmosphere, due to the lower air pres-
85 sure that increases static stability. The stability Iris hypothesis states that the increased
86 stability reduces the magnitude of the radiatively-driven clear-sky mass convergence at
87 the height of anvil clouds, thus weakening convective detrainment at that height, lead-
88 ing to a reduction of the anvils coverage. Several climate models and convection-resolving
89 models have provided support for this hypothesis (Zelinka & Hartmann, 2010; Bony et
90 al., 2016; Cronin & Wing, 2017), but the existence of the stability Iris effect in Nature
91 remains an open question.

92 To investigate the existence of the stability Iris effect in observations, we use lidar
93 observations derived from the A-train Cloud-Aerosol Lidar and Infrared Pathfinder Satel-
94 lite Observations CALIPSO (Stephens et al., 2017; Winker et al., 2017), together with
95 ERA5 meteorological reanalyses (Hersbach et al., 2019). Lidar measurements from CALIPSO
96 provide the most accurate cloud vertical profile measurements without time drift (Winker
97 et al., 2007, 2017) and on a very fine vertical resolution (60 m). Here we use 10 years
98 of data, that include two El Niño and three La Niña events, to examine the behavior of
99 the anvil cloud fraction as the tropics undergo warming or cooling events. In order to
100 test the robustness of our results, and to determine whether they could emerge at coarser
101 vertical resolutions of climate models, we also use the GCM-oriented CALIPSO Cloud
102 Product GOCCP (Chepfer et al., 2010). We further investigate the existence of PHAT
103 in these observations, as well as the spatial scale at which PHAT and the stability Iris
104 potentially hold.

105 **2 Data and methods**

106 **2.1 Detection of anvils in CALIPSO observations**

107 In this study, we refer to anvils as the detraining top of deep convective clouds, which
108 lie above 8 km in the tropics (Yuan et al., 2011). To identify tropical anvils, we use the
109 monthly-mean three dimensional cloud fraction derived from the lidar level 3 cloud oc-
110 currence product (CAL_LID_L3_Cloud_Occurrence-Standard-V1-00, Winker (2018)), here-
111 after CALIPSO-Cloud-Occurrence. CALIPSO-Cloud-Occurrence is gridded on 2° lat-

112 altitude $\times 2.5^\circ$ longitude and on the native CALIOP vertical resolution of 60 m (344 ver-
 113 tical levels). We use it over the tropical belt (30N-30S), averaged over day and night,
 114 from June 2006 to December 2016 (10 years). CALIPSO-Cloud-Occurrence is used through-
 115 out the study except for what is related to Figure 4b in section 4.1, where results are repli-
 116 cated using GOCCP instead (Chepfer et al., 2010), which provides the monthly-mean
 117 cloud fraction gridded on a $2^\circ \times 2^\circ$ horizontal grid with a degraded vertical resolution of
 118 480 m (40 vertical levels), from June 2006 to December 2017 (11 years). In this case, GOCCP
 119 is used to determine whether our results can emerge at coarser vertical resolutions of Gen-
 120 eral Circulation Models (GCMs), indicating whether the ability of climate models to re-
 121 produce these results can be tested.

122 For each month and location ($2^\circ \times 2.5^\circ$ gridbox), we define the altitude and the cloud
 123 fraction of anvil clouds, resp. Z_{anv} and CF_{anv} , where there is a local maximum of op-
 124 tically thick but non-opaque ice clouds coverage (optical depth $0.3 \leq \tau < 5$), impos-
 125 ing that this maximum occurs above 8 km and that its cloud fraction exceeds a thresh-
 126 old value referred to as CF_c (we use $CF_c = 0.03$). If there are several local maxima,
 127 we consider the closest to the cloud fraction centroid. Locations that are cloud-free or
 128 where no maximum exceeds CF_c are masked and ignored when tropically-averaging Z_{anv}
 129 or CF_{anv} . With CALIPSO-Cloud-Occurrence only, local maxima are identified from the
 130 smoothed cloud fraction profile, using a 480-meters running window (smoothing is only
 131 used for this purpose). Note that our results do not critically depend on the method used
 132 to locate the anvils altitude (not shown).

133 This definition of anvils excludes clear-sky regions and regions with a low cloud frac-
 134 tion, as well as subvisible cirrus clouds, and the cores of deep convective clouds. These
 135 choices will be tested and discussed in section 4. As will be shown, the conclusions of
 136 this study do not critically depend on the value of CF_c , nor on the exact range of op-
 137 tical depths considered. Figure 1a shows the annual-mean cloud fraction profile averaged
 138 over locations where anvils have been detected (locations void of anvils are ignored), within
 139 the tropical belt (30N-30S), considering thick but non-opaque ice clouds with $CF_{anv} \geq$
 140 0.03.

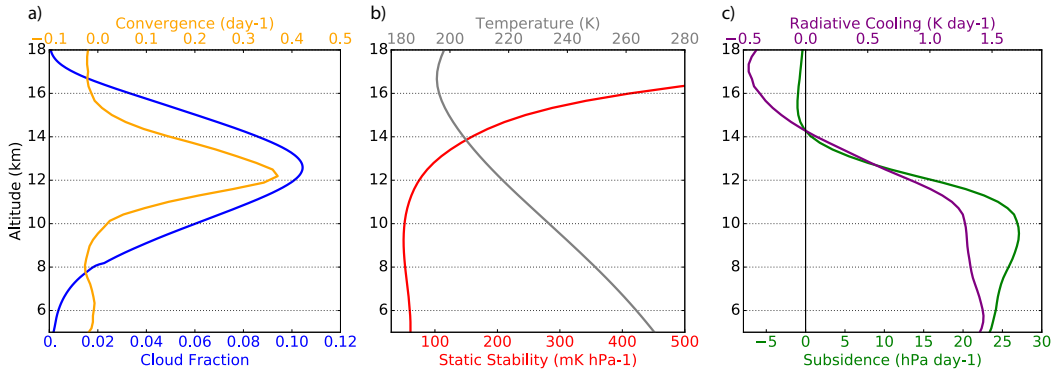


Figure 1. Vertical profiles, averaged over the tropics and over 2006-2016, of: a) cloud fraction averaged over locations with anvils only (blue) and radiatively-driven clear-sky mass convergence ($\partial\omega_r/\partial p$, orange), b) atmospheric static stability (S , red) and temperature (grey), c) clear-sky radiative cooling (Q_r , purple) and radiatively-driven clear-sky pressure velocity (ω_r , green).

141 **2.2 Clear-sky variables from ERA5**

142 According to PHAT, anvils form at the altitude of the peak of upper-tropospheric
 143 horizontal mass divergence in convective regions, which coincides with a peak of radiatively-

144 driven mass convergence in clear-sky regions (Hartmann & Larson, 2002; Zelinka & Hart-
 145 mann, 2010). The radiatively-driven clear-sky pressure velocity (ω_r , positive downward)
 146 and divergence (D_r) are diagnosed as:

$$D_r = \max\left(\frac{\partial\omega_r}{\partial p}\right), \text{ with } \omega_r = \frac{Q_r}{S} \text{ and } S = \frac{T}{p} \frac{R}{c_p} - \frac{\partial T}{\partial p} \quad (1)$$

147 where Q_r is the clear-sky radiative cooling rate, p the air pressure, S the static sta-
 148 bility, T the temperature, R the gas constant, c_p the isobaric specific heat of dry air.

149 We use monthly mean clear-sky radiative cooling, temperature and pressure from
 150 ERA5 reanalyses in the tropics, horizontally regridded onto the CALIPSO-Cloud-Occurrence
 151 $2^\circ \times 2.5^\circ$ grid, with a vertical resolution of about 300 m in the upper troposphere (137 ver-
 152 tical levels in the whole atmosphere), from June 2006 to December 2017. We compute
 153 the peak of upper-tropospheric horizontal mass divergence at each month and location,
 154 which is simply defined as its maximum. The altitude of this peak is referred to as Z_{D_r} .

155 Figures 1b and 1c show that the annual-mean tropically-averaged Q_r (in purple)
 156 weakens in the upper-troposphere above 10 km, while S (in red) sharply increases above
 157 12 km. As a consequence, the radiatively-driven clear-sky subsidence (ω_r , in green) weak-
 158 ens above 10 km. Following this, Figure 1a shows that the radiatively-driven clear-sky
 159 mass convergence ($\partial\omega_r/\partial p$, in orange) peaks near 12 km, at about 216 K (Fig. 1b), and
 160 the anvils cloud fraction profile (in blue) peaks near 12.5 km, at about 214 K. The anvils
 161 cloud fraction profile thus exhibits a clear correspondence with the radiatively-driven clear-
 162 sky mass convergence profile.

163 2.3 Surface temperatures from HadCRUT4

164 Monthly land and sea surface temperatures (T_s) are derived from HadCRUT4 (Morice
 165 et al., 2012) in the tropics, from June 2006 to December 2017. The Oceanic Niño Index
 166 (ONI, Golden Gate Weather Services) indicates that the 11-year period, or the 10-year
 167 period from 2006 to 2016, includes one strong (2009-2010) and one very strong (2015-
 168 2016) El Niño events, two strong (2007-2008, 2010-2011) and one moderate (2011-2012)
 169 La Niña events. El Niño years correspond to the highest tropical-mean surface temper-
 170 ature and La Niña years to the lowest.

171 3 Evidence for PHAT and the stability Iris effect

172 We consider yearly means, computed by averaging each year from July to June,
 173 in order to capture the response to El Niño/La Niña-induced surface temperature changes,
 174 that will be maximum during boreal winter (we compute tropically-averaged yearly anoma-
 175 lies as $\langle \bar{x} \rangle_{year} - \langle \bar{x} \rangle_{2006-2016}$, where the overbar denotes tropical averaging, brackets de-
 176 note time averaging, $year$ refers to each year within 2006-2016, and x can be Z_{anv} , T_s ,
 177 Z_{D_r} , or other variables).

178 On the tropical and interannual scales, strong correlations of Z_{anv} and Z_{D_r} with
 179 the tropical-mean surface temperature confirm that both anvils and D_r rise as the trop-
 180 ics warm ($r = 0.87$ and $r = 0.94$, respectively, Figures 2a and 2b). The altitudes of
 181 both anvils and D_r are the highest during the very strong 2015-2016 El Niño, relative
 182 to the rest of the 10-year record, with anvils forming about 100 m higher than on av-
 183 erage (Figure 2a). During that very strong El Niño year, the air temperature at around
 184 12 km increased by about 0.84 K relative to the 10-year average, while the anvils tem-
 185 perature remained at approximately the same temperature, changing by only 0.006 K
 186 (not shown). The altitude of anvils varies in phase with the altitude of the divergence
 187 peak D_r , as shown by the correlation of $r = 0.95$ between Z_{anv} and Z_{D_r} , with a slope
 188 that is not statistically different from 1 (Figure 2c). All these findings support the PHAT

189 hypothesis. Note that models rather predict that anvils migrate more than the diver-
 190 gence peak (Zelinka & Hartmann, 2010).

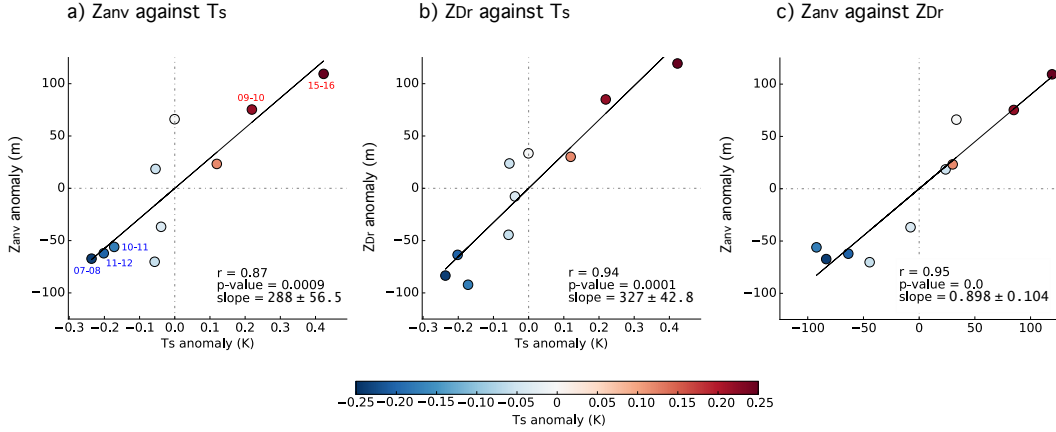


Figure 2. Scatterplots showing tropically-averaged yearly anomalies (each dot is a July-to-June year, anomalous relative to the time-mean over 2006-2016). Linear regressions are also reported (black lines) together with the Pearson correlation coefficient r , the p -value and the slope. Colors show the tropical-mean surface temperature anomaly and numbers in (a) give the corresponding year of El Niño (red) and La Niña (blue) events. The relationships involve the anvils altitude Z_{anv} , the tropical surface temperature T_S and the divergence peaks altitude Z_{D_r} .

191 In addition to PHAT, Figure 3a shows that tropical warming is associated with a
 192 reduced anvils coverage (negative correlation between CF_{anv} and T_s , $r = -0.97$). This
 193 supports the existence of an Iris effect, as defined by a reduction of anvils coverage as-
 194 sociated with tropical warming.

195 Moreover, the decrease of anvils coverage is associated with a weakening of the ra-
 196 diative divergence peak D_r , as shown by the correlation between CF_{anv} and D_r of $r =$
 197 0.84 (Figure 3b). This supports the idea that anvils are tightly linked to the peak of the
 198 radiatively-driven clear-sky convergence: not only their altitudes but also their ampli-
 199 tudes vary in phase.

200 As the clear-sky radiative cooling profile (Q_r) shifts upward, the vertical gradient
 201 of the radiatively-driven subsidence ($\partial\omega_r/\partial p$) becomes less steep because of the stronger
 202 stability (S), which weakens the divergence peak D_r (Eq. 1). This is supported by the
 203 negative correlation between D_r and the stability at the level of D_r (S_{D_r}), of $r = -0.82$
 204 (Figure 3c). This all happens in response to tropical warming, as shown by the correlation
 205 between S_{D_r} and T_s of $r = 0.89$ (Figure 3d). To summarize, the reduction of both
 206 D_r and CF_{anv} is associated with an increase of static stability at the height of anvils,
 207 in response to tropical warming. Although causality cannot be determined from obser-
 208 vations, these relationships are fully consistent with the stability Iris mechanism.

209 4 Spatial scale and robustness of the observed relationships

210 4.1 Varying spatial scale, critical anvil cloud fraction and vertical res- 211 olution

212 To test the robustness of our results, we assess the sensitivity of the PHAT rela-
 213 tionships shown on Figures 2a and 2c (Z_{anv} against T_S and against Z_{D_r}), the Iris effect
 214 and the stability Iris effect relationships shown on Figures 3a and 3b (CF_{anv} against T_S

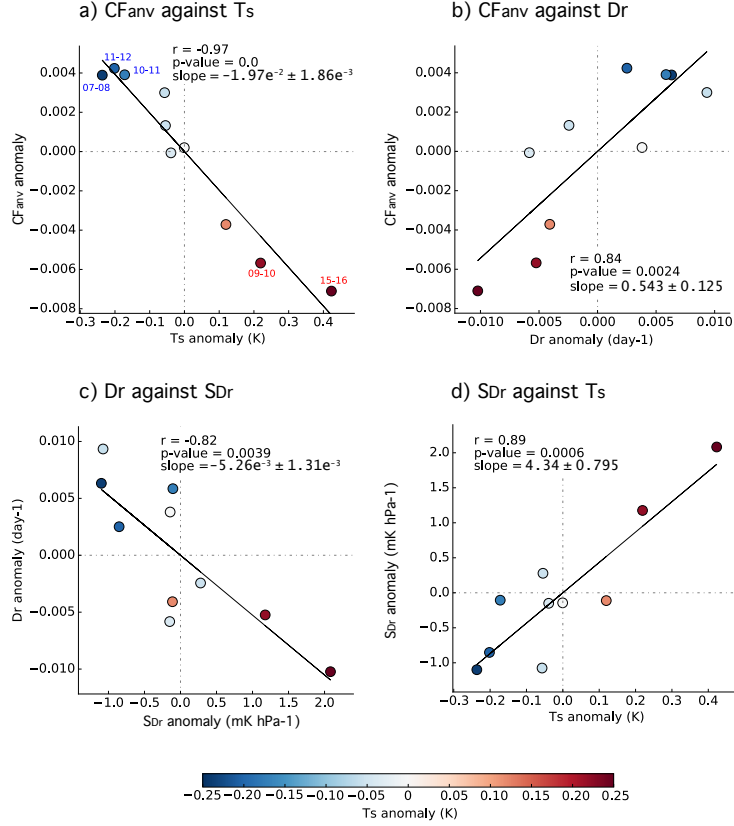


Figure 3. As Figure 2, but for other relationships involving the anvils cloud fraction CF_{anv} , the divergence peak D_r , the tropical-mean surface temperature T_s and the stability at D_r level (S_{D_r}).

215 and against D_r), to the value of the CF_c threshold used to identify anvils. Figure 4a shows
 216 that all relationships remain strong ($|r| \geq 0.7$) and significant ($p\text{-value} < 0.05$) for CF_c
 217 ranging from 0 to 0.13.

218 PHAT and the stability Iris hypothesis relate the altitude and coverage of anvils
 219 to the radiatively-driven convergence in surrounding clear-sky regions. However, the scale
 220 of this “surrounding” is unclear. Thompson et al. (2017) observed that PHAT holds on
 221 zonal averages at each latitude. This leads to the following question: over which spatial
 222 scale does the balance between clear-sky convergence and convective detrainment hold?

223 To answer this question, we use the different values of CF_c tested above, because
 224 they affect the tropical coverage of identified anvils. For example, $CF_c = 0$ (i.e. $CF_{anv} >$
 225 0) means that anvils are defined where there is a cloud fraction maximum in the upper
 226 troposphere without any constraint on the magnitude of this maximum (in this case anvils
 227 are present in about 83% of the $2^\circ \times 2.5^\circ$ grid-points of the tropics on average), while $CF_c =$
 228 0.13 (i.e. $CF_{anv} \geq 0.13$) means that anvils are only detected where the cloud fraction
 229 maximum in the upper troposphere exceeds 0.13 (represents about 30% of the $2^\circ \times 2.5^\circ$
 230 grid-points of the tropics on average, Figure 4a). On the other hand, the clear-sky re-
 231 gions (hence D_r and Z_{D_r}) are so far considered over the whole tropical belt in all cases
 232 (30N-30S). The PHAT, Iris and stability Iris relationships are thus already shown to be
 233 well observed at the tropics scale, since they remain strong even when some clear-sky
 234 regions are remote from the identified anvils (for all values of CF_c).

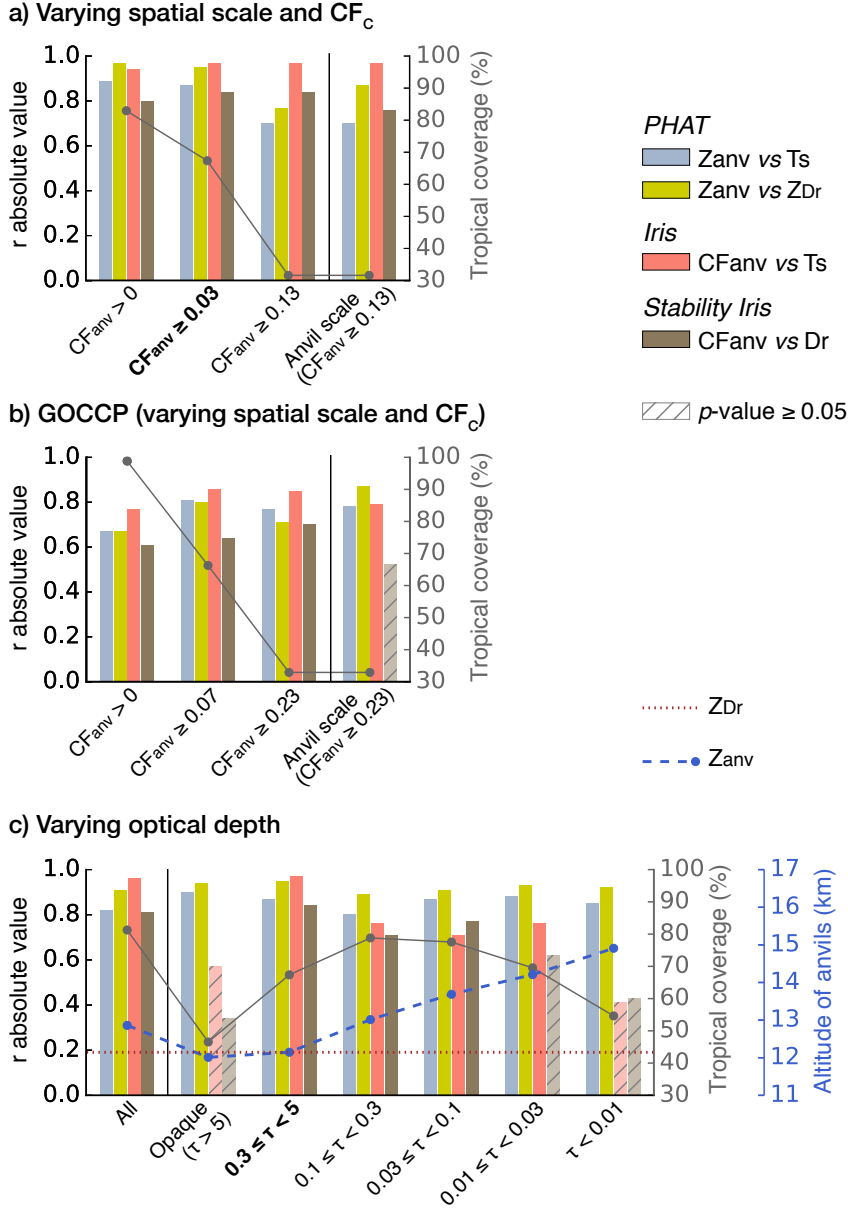


Figure 4. Evolution of linear regressions shown on Figures 2a, 2c, 3a and 3b with varying the spatial scale and critical cloud fraction CF_c , with Calipso-Cloud-Occurrence (a) and GOCCP (b), and with varying optical depths of selected anvils (c). Color bars give the absolute value of the Pearson correlation coefficients r . Hatched light bars indicate that p -value ≥ 0.05 . The grey line gives the average percentage of the tropics covered by identified anvils. a, b) The last case (Anvil scale) is when the definition of T_S , D_r and Z_{D_r} is restricted to locations with anvils. c) Only clouds of a certain range of optical depths (τ) are considered, above 8 km: all clouds (ice and water), ice opaque clouds, and ice non-opaque clouds within different τ ranges. The dashed blue line gives the average altitude of selected anvils Z_{anv} in annual-mean. The dotted brown horizontal line indicates the annual-mean value of Z_{D_r} , averaged over the whole tropics. a, c) Categories in bold correspond to the results shown in section 3.

235 We now restrict the definition of the clear-sky surroundings to the immediate vicinity
 236 of anvils which exceed a strong cloud fraction threshold, by computing D_r and Z_{D_r}
 237 only on locations where anvils have been detected with $CF_{anv} \geq 0.13$ (the surface tem-
 238 perature is also considered only on these same locations). In this case, we choose the strongest
 239 CF_c threshold because it corresponds to the smallest scale we can investigate, as most
 240 clear-sky regions are then remote from the identified anvils. These remote clear-sky re-
 241 gions are thus fully ignored and relationships can be examined at the anvil scale (or lo-
 242 cal scale). The corresponding correlation coefficients are shown on Figure 4a at the ex-
 243 treme right of the plot, and remain strong and significant for all four relationships. The
 244 same results are obtained when using the total cloud fraction (that is, not restricting to
 245 ice thick non-opaque clouds), with all correlations remaining strong and significant for
 246 the whole range of spatial scales (not shown). The PHAT, Iris and stability Iris relation-
 247 ships thus hold both at the large scale, such as those of the Hadley-Walker circulations,
 248 and at the scale of the close surroundings of the anvils, within a few hundred kilometers.

249 We now replicate this analysis with the GCM-oriented GOCCP product, which de-
 250 tects and diagnoses the total cloud fraction assuming a coarser vertical resolution of the
 251 lidar backscatter signal, of 480 m instead of 60 m. Here again, depending on the CF_c
 252 threshold used to define anvils, anvils cover either 99% (with $CF_{anv} > 0$), or about 70%
 253 (with $CF_{anv} \geq 0.07$), or about 30% (with $CF_{anv} \geq 0.23$) of the $2^\circ \times 2^\circ$ grid-points of
 254 the tropics on average (Figure 4b). Although all four correlations weaken with GOCCP,
 255 they are still significant when anvils cover 99%, 70% or 30% of the tropics ($|r| > 0.6$).
 256 Only at the anvil scale, where clear-sky regions are restricted to the immediate vicini-
 257 ty of anvils selected with a strong threshold ($CF_{anv} \geq 0.23$), evidence of the stabil-
 258 ity Iris effect becomes faint but is still detectable ($r = 0.52$ with p -value = 0.0992). There-
 259 fore the PHAT, Iris and stability Iris relationships remain detectable with a degraded
 260 vertical resolution of about 500 m, although with better significance when clear-sky re-
 261 gions encompass more than the immediate vicinity of anvils.

262 4.2 Influence of the anvils optical depth

263 So far, our definition of anvil clouds has been restricted to thick but non-opaque
 264 ice clouds ($0.3 \leq \tau < 5$). Figure 4c compares the correlation coefficients for the PHAT,
 265 Iris and stability Iris relationships when using a range of optical depths. Note that the
 266 value of CF_c is adapted in each case to remain proportional to the maximum of the annual-
 267 mean tropically-averaged cloud fraction profile; practically $CF_c = 0.42 \times \max(\langle \overline{CF} \rangle)$.
 268 As the optical depth decreases, the altitude of the selected clouds increases, going up to
 269 15 km for thin ice clouds ($\tau < 0.01$), consistent with the persistent occurrence of sub-
 270 visible cirrus clouds near the tropical tropopause (e.g. Wang et al. (1994); Jensen et al.
 271 (1996, 1999)). On the other hand, the altitude of opaque ice clouds, which correspond
 272 to the cores of deep convective clouds, is around 12 km.

273 The PHAT relationships remain strong and significant for all optical depths ($r >$
 274 0.7), meaning that the altitude of all high clouds (opaque, thick or thin) is correlated
 275 with T_S and Z_{D_r} . PHAT thus seems to hold for anvils as well as for high cirrus clouds,
 276 which is consistent with the vertical structure of the atmosphere, including cirrus clouds
 277 near the tropopause, rising approximately in step with the atmospheric isotherms as the
 278 tropics warm (Gage & Reid, 1986; Lu et al., 2008).

279 The Iris and stability Iris relationships remain strong and significant for most non-
 280 opaque ice clouds ($|r| > 0.7$ for $\tau \geq 0.03$), except for high subvisible cirrus clouds ($|r| <$
 281 0.5 for $\tau < 0.01$). This suggests that the cloud fraction of subvisible clouds is dominated
 282 by in-situ cirrus clouds, which form when ice condensates near the tropopause rather than
 283 being directly injected from deep convection, regardless of the stability Iris effect. The
 284 Iris and stability Iris relationships are also weak and non-significant for ice opaque clouds
 285 ($0.5 < |r| < 0.6$ for Iris and $r < 0.4$ for stability Iris), which are found at the deepest

286 cores of convective systems (as suggested by their relatively low altitude, tropical cov-
 287 erage and strong optical depth). This suggests that the cloud fraction of deep convec-
 288 tive cores is less constrained by the upper-tropospheric clear-sky mass divergence than
 289 the cloud fraction of detrained anvils. Following this, the ratio of CF_{anv} for opaque ice
 290 clouds to CF_{anv} for thick but non-opaque ice clouds ($0.3 \leq \tau < 5$) is the greatest (0.88)
 291 during the hottest 2015-2016 El Niño year, and the second lowest (0.83) during the cold-
 292 est 2007-2008 La Niña year, although there is no correlation with T_S on the 10-year pe-
 293 riod (not shown).

294 5 Conclusions

295 Interannual variations of the anvils cloud fraction, inferred from 10 years of CALIPSO
 296 measurements, show that the anvils coverage is reduced when the tropics are anomalously
 297 warm. ERA5 reanalyses further show that the altitude and extent of anvils vary in phase
 298 with the altitude and strength of the radiatively-driven clear-sky mass convergence peak,
 299 and that both are tightly linked to the static stability profile. As the tropics warm, the
 300 peak of the clear-sky radiatively-driven mass convergence rises, and weakens because of
 301 the increase in stability with height, resulting in a reduced anvil cloud fraction. High sub-
 302 visible cirrus clouds and deep-convective clouds also rise in step with temperature, but
 303 only the cloud fraction of anvil clouds is reduced with warming, consistent with the sta-
 304 bility Iris effect. Robust, consistent and highly significant relationships derived from 10 years
 305 of CALIPSO observations provide a strong observational support for both the PHAT and
 306 the stability Iris hypotheses. Observations further show that PHAT and the stability Iris
 307 effect hold over a large range of spatial scales. This suggests that clear-sky regions can
 308 influence anvils both in the vicinity of clouds and remotely over long distances.

309 At the interannual scale, tropical warming anomalies generally coincide with El Niño
 310 events. Although the interannual and the longer-term climate change responses to trop-
 311 ical warming cannot be directly compared, theoretically PHAT and the stability Iris ef-
 312 fect can hold in both contexts. Whether or not the relationship with temperature shown
 313 here actually applies to longer-term global warming, remains an open question. Beyond
 314 surface warming, anthropogenically-induced changes in upper-tropospheric CO_2 and ozone
 315 concentrations might change the static stability profile, and thus potentially overwhelm
 316 the stability Iris effect (Harrop & Hartmann, 2012). CO_2 -induced changes in the atmo-
 317 spheric overturning circulation (Bony et al., 2013) could also influence the altitude and
 318 coverage of tropical anvils. The continuation of spaceborne lidar measurements on the
 319 long term will allow us to monitor these changes. Although the evidence for the stabil-
 320 ity Iris effect is stronger when using highly vertically-resolved lidar measurements, it re-
 321 mains when using data at coarser vertical resolutions. This suggests that GOCCP could
 322 be used to test the ability of climate models to reproduce this effect. This will consti-
 323 tute a necessary, albeit not sufficient, test of the credibility of the predicted behavior of
 324 anvil clouds with temperature in the models.

325 Finally, we emphasize that the stability Iris hypothesis does not imply anything
 326 about the radiative impact of the anvils behavior. The rise of anvils with warming is known
 327 to produce a positive climate feedback (Zelinka & Hartmann, 2010). The decrease of anvils
 328 coverage with warming can be associated with both an increase in the outgoing longwave
 329 radiation and a decrease in planetary albedo. It can also enhance the exposure to space
 330 of low-level clouds, which may also impact the overall planetary albedo. Whether one
 331 effect dominates over the other is unknown a priori, and will require a specific study.

Acknowledgments

We thank the two anonymous reviewers for their suggestions, which helped to substantially improve the manuscript. MSL is funded by the CNES (Centre National d'Études Spatiales). SB and JLD are supported by the European Union's Horizon 2020 research and innovation program under grant agreements No 694768 (ERC project EUREC4A) and No 820829 (CONSTRAIN project). To process the CALIPSO, GOCCP and ERA5 data, this study benefited from the IPSL mesocenter ESPRI facility which is supported by CNRS, Sorbonne Université, Labex L-IPSL, CNES and Ecole Polytechnique. We acknowledge Copernicus Climate Change Service (C3S) (2017) for ERA5 (Fifth generation of ECMWF atmospheric reanalyses of the global climate): <https://cds.climate.copernicus.eu/cdsapp#!/home>. CALIPSO level 3 cloud occurrence data is available at: https://eosweb.larc.nasa.gov/project/calipso/cal_lid_l3_cloud_occurrence_v1-00. GOCCP data is available at: https://climserv.ipsl.polytechnique.fr/cfmip-obs/Calipso_goccp.html. The Met Office HadCRUT4 product is available at: <https://www.metoffice.gov.uk/hadobs/hadcrut4/>.

References

- Bony, S., Bellon, G., Klocke, D., Sherwood, S., Fermepin, S., & Denvil, S. (2013, June). Robust direct effect of carbon dioxide on tropical circulation and regional precipitation. *Nature Geoscience*, *6*(6), 447–451. Retrieved 2013-09-30, from <http://www.nature.com/ngeo/journal/v6/n6/full/ngeo1799.html> doi: 10.1038/ngeo1799
- Bony, S., Stevens, B., Coppin, D., Becker, T., Reed, K. A., Voigt, A., & Medeiros, B. (2016, September). Thermodynamic control of anvil cloud amount. *Proceedings of the National Academy of Sciences*, *113*(32), 8927–8932. Retrieved 2017-10-10, from <http://www.pnas.org/content/113/32/8927> doi: 10.1073/pnas.1601472113
- Bony, S., Stevens, B., Frierson, D. M. W., Jakob, C., Kageyama, M., Pincus, R., ... Webb, M. J. (2015, March). Clouds, circulation and climate sensitivity. *Nature Geoscience*, *8*(4), ngeo2398. Retrieved 2017-11-10, from <https://www.nature.com/articles/ngeo2398> doi: 10.1038/ngeo2398
- Chepfer, H., Bony, S., Winker, D., Cesana, G., Dufresne, J. L., Minnis, P., ... Zeng, S. (2010, February). The GCM-Oriented CALIPSO Cloud Product (CALIPSO-GOCCP). *Journal of Geophysical Research: Atmospheres*, *115*(D4), D00H16. Retrieved 2017-11-15, from <http://onlinelibrary.wiley.com/doi/10.1029/2009JD012251/abstract> doi: 10.1029/2009JD012251
- Choi, Y.-S., Kim, W., Yeh, S.-W., Masunaga, H., Kwon, M.-J., Jo, H.-S., & Huang, L. (2017, June). Revisiting the iris effect of tropical cirrus clouds with TRMM and A-Train satellite data. *Journal of Geophysical Research: Atmospheres*, *122*(11), 2016JD025827. Retrieved 2018-02-11, from <http://onlinelibrary.wiley.com/doi/10.1002/2016JD025827/abstract> doi: 10.1002/2016JD025827
- Cronin, T. W., & Wing, A. A. (2017, December). Clouds, Circulation, and Climate Sensitivity in a Radiative-Convective Equilibrium Channel Model. *Journal of Advances in Modeling Earth Systems*, *9*(8), 2883–2905. Retrieved 2018-03-09, from <http://onlinelibrary.wiley.com/doi/10.1002/2017MS001111/abstract> doi: 10.1002/2017MS001111
- Del Genio, A. D., & Kovari, W. (2002, September). Climatic Properties of Tropical Precipitating Convection under Varying Environmental Conditions. *Journal of Climate*, *15*(18), 2597–2615. Retrieved 2018-03-09, from [https://journals.ametsoc.org/doi/abs/10.1175/1520-0442\(2002\)015%3C2597:CPOTPC%3E2.0.CO%3B2](https://journals.ametsoc.org/doi/abs/10.1175/1520-0442(2002)015%3C2597:CPOTPC%3E2.0.CO%3B2) doi: 10.1175/1520-0442(2002)015<2597:CPOTPC>2.0.CO;2
- Eitzen, Z. A., Xu, K.-M., & Wong, T. (2009, November). Cloud and Radiative

- 385 Characteristics of Tropical Deep Convective Systems in Extended Cloud Ob-
 386 jects from CERES Observations. *Journal of Climate*, 22(22), 5983–6000.
 387 Retrieved 2019-07-25, from [https://journals.ametsoc.org/doi/full/](https://journals.ametsoc.org/doi/full/10.1175/2009JCLI3038.1)
 388 [10.1175/2009JCLI3038.1](https://journals.ametsoc.org/doi/full/10.1175/2009JCLI3038.1) doi: 10.1175/2009JCLI3038.1
- 389 Gage, K. S., & Reid, G. C. (1986). The tropical tropopause and the El
 390 Niño of 1982–1983. *Journal of Geophysical Research: Atmospheres*,
 391 91(D12), 13315–13317. Retrieved 2020-05-20, from [https://agupubs](https://agupubs.onlinelibrary.wiley.com/doi/abs/10.1029/JD091iD12p13315)
 392 [.onlinelibrary.wiley.com/doi/abs/10.1029/JD091iD12p13315](https://agupubs.onlinelibrary.wiley.com/doi/abs/10.1029/JD091iD12p13315) (_eprint:
 393 <https://agupubs.onlinelibrary.wiley.com/doi/pdf/10.1029/JD091iD12p13315>)
 394 doi: 10.1029/JD091iD12p13315
- 395 Harrop, B. E., & Hartmann, D. L. (2012, March). Testing the Role of Radiation
 396 in Determining Tropical Cloud-Top Temperature. *Journal of Climate*, 25(17),
 397 5731–5747. Retrieved 2019-06-18, from [https://journals.ametsoc.org/doi/](https://journals.ametsoc.org/doi/full/10.1175/JCLI-D-11-00445.1)
 398 [full/10.1175/JCLI-D-11-00445.1](https://journals.ametsoc.org/doi/full/10.1175/JCLI-D-11-00445.1) doi: 10.1175/JCLI-D-11-00445.1
- 399 Hartmann, D. L. (2016, August). Tropical anvil clouds and climate sensitiv-
 400 ity. *Proceedings of the National Academy of Sciences*, 113(32), 8897–8899.
 401 Retrieved 2019-12-04, from [http://www.pnas.org/lookup/doi/10.1073/](http://www.pnas.org/lookup/doi/10.1073/pnas.1610455113)
 402 [pnas.1610455113](http://www.pnas.org/lookup/doi/10.1073/pnas.1610455113) doi: 10.1073/pnas.1610455113
- 403 Hartmann, D. L., & Larson, K. (2002, October). An important constraint on trop-
 404 ical cloud - climate feedback. *Geophysical Research Letters*, 29(20), 1951.
 405 Retrieved 2017-10-10, from [http://onlinelibrary.wiley.com/doi/10.1029/](http://onlinelibrary.wiley.com/doi/10.1029/2002GL015835/abstract)
 406 [2002GL015835/abstract](http://onlinelibrary.wiley.com/doi/10.1029/2002GL015835/abstract) doi: 10.1029/2002GL015835
- 407 Hartmann, D. L., & Michelsen, M. L. (2002, February). No evidence for iris.
 408 *Bulletin of the American Meteorological Society*, 83(2), 249–254. Re-
 409 trieved 2018-03-09, from [https://journals.ametsoc.org/doi/abs/](https://journals.ametsoc.org/doi/abs/10.1175/1520-0477(2002)083%3C0249%3ANEFI%3E2.3.CO;2)
 410 [10.1175/1520-0477\(2002\)083%3C0249%3ANEFI%3E2.3.CO;2](https://journals.ametsoc.org/doi/abs/10.1175/1520-0477(2002)083%3C0249%3ANEFI%3E2.3.CO;2) doi: 10.1175/
 411 [1520-0477\(2002\)083\(0249:NEFI\)2.3.CO;2](https://journals.ametsoc.org/doi/abs/10.1175/1520-0477(2002)083%3C0249%3ANEFI%3E2.3.CO;2)
- 412 Hersbach, H., Bell, B., Berrisford, P., Horányi, A., Muñoz Sabater, J., Nicolas, J., ...
 413 others (2019, April). Global reanalysis: goodbye ERA-Interim, hello ERA5,
 414 ECMWF Newsletter, No. 159, ECMWF. *ECMWF Newsletter*(159), 17–24.
- 415 Jensen, E. J., Read, W. G., Mergenthaler, J., Sandor, B. J., Pfister, L.,
 416 & Tabazadeh, A. (1999). High humidities and subvisible cir-
 417 rus near the tropical tropopause. *Geophysical Research Letters*,
 418 26(15), 2347–2350. Retrieved 2020-05-13, from [https://agupubs](https://agupubs.onlinelibrary.wiley.com/doi/abs/10.1029/1999GL900266)
 419 [.onlinelibrary.wiley.com/doi/abs/10.1029/1999GL900266](https://agupubs.onlinelibrary.wiley.com/doi/abs/10.1029/1999GL900266) (_eprint:
 420 <https://agupubs.onlinelibrary.wiley.com/doi/pdf/10.1029/1999GL900266>) doi:
 421 [10.1029/1999GL900266](https://agupubs.onlinelibrary.wiley.com/doi/pdf/10.1029/1999GL900266)
- 422 Jensen, E. J., Toon, O. B., Selkirk, H. B., Spinhirne, J. D., & Schoeberl, M. R.
 423 (1996). On the formation and persistence of subvisible cirrus clouds
 424 near the tropical tropopause. *Journal of Geophysical Research: Atmo-*
 425 *spheres*, 101(D16), 21361–21375. Retrieved 2020-05-13, from [https://](https://agupubs.onlinelibrary.wiley.com/doi/abs/10.1029/95JD03575)
 426 agupubs.onlinelibrary.wiley.com/doi/abs/10.1029/95JD03575 (_eprint:
 427 <https://agupubs.onlinelibrary.wiley.com/doi/pdf/10.1029/95JD03575>) doi:
 428 [10.1029/95JD03575](https://agupubs.onlinelibrary.wiley.com/doi/pdf/10.1029/95JD03575)
- 429 Khairoutdinov, M., & Emanuel, K. (2013). Rotating radiative-convective equilib-
 430 rium simulated by a cloud-resolving model. *Journal of Advances in Modeling*
 431 *Earth Systems*, 5(4), 816–825. Retrieved 2019-11-25, from [https://agupubs](https://agupubs.onlinelibrary.wiley.com/doi/abs/10.1002/2013MS000253)
 432 [.onlinelibrary.wiley.com/doi/abs/10.1002/2013MS000253](https://agupubs.onlinelibrary.wiley.com/doi/abs/10.1002/2013MS000253) doi: 10.1002/
 433 [2013MS000253](https://agupubs.onlinelibrary.wiley.com/doi/abs/10.1002/2013MS000253)
- 434 Kubar, T. L., Hartmann, D. L., & Wood, R. (2007, November). Radiative and
 435 Convective Driving of Tropical High Clouds. *Journal of Climate*, 20(22), 5510–
 436 5526. Retrieved 2019-07-25, from [https://journals.ametsoc.org/doi/full/](https://journals.ametsoc.org/doi/full/10.1175/2007JCLI1628.1)
 437 [10.1175/2007JCLI1628.1](https://journals.ametsoc.org/doi/full/10.1175/2007JCLI1628.1) doi: 10.1175/2007JCLI1628.1
- 438 Li, Y., Yang, P., North, G. R., & Dessler, A. (2012, February). Test of the Fixed
 439 Anvil Temperature Hypothesis. *Journal of the Atmospheric Sciences*, 69(7),

- 2317–2328. Retrieved 2019-07-25, from <https://journals.ametsoc.org/doi/full/10.1175/JAS-D-11-0158.1> doi: 10.1175/JAS-D-11-0158.1
- Lindzen, R. S., Chou, M.-D., & Hou, A. Y. (2001, March). Does the Earth Have an Adaptive Infrared Iris? *Bulletin of the American Meteorological Society*, 82(3), 417–432. Retrieved 2018-02-13, from <https://journals.ametsoc.org/doi/abs/10.1175/1520-0477%282001%29082%3C0417%3ADTEHAA%3E2.3.CO%3B2> doi: 10.1175/1520-0477(2001)082(0417:DTEHAA)2.3.CO;2
- Liu, R., Liou, K.-N., Su, H., Gu, Y., Zhao, B., Jiang, J. H., & Liu, S. C. (2017). High cloud variations with surface temperature from 2002 to 2015: Contributions to atmospheric radiative cooling rate and precipitation changes. *Journal of Geophysical Research: Atmospheres*, 122(10), 5457–5471. Retrieved 2019-06-25, from <https://agupubs.onlinelibrary.wiley.com/doi/abs/10.1002/2016JD026303> doi: 10.1002/2016JD026303
- Lu, J., Chen, G., & Frierson, D. M. W. (2008, November). Response of the Zonal Mean Atmospheric Circulation to El Niño versus Global Warming. *Journal of Climate*, 21(22), 5835–5851. Retrieved 2020-05-20, from <https://journals.ametsoc.org/doi/full/10.1175/2008JCLI2200.1> (Publisher: American Meteorological Society) doi: 10.1175/2008JCLI2200.1
- Mauritsen, T., & Stevens, B. (2015, May). Missing iris effect as a possible cause of muted hydrological change and high climate sensitivity in models. *Nature Geoscience*, 8(5), 346–351. Retrieved 2019-02-07, from <https://www.nature.com/articles/ngeo2414> doi: 10.1038/ngeo2414
- Morice, C. P., Kennedy, J. J., Rayner, N. A., & Jones, P. D. (2012, April). Quantifying uncertainties in global and regional temperature change using an ensemble of observational estimates: The HadCRUT4 data set: THE HADCRUT4 DATASET. *Journal of Geophysical Research: Atmospheres*, 117(D8), n/a–n/a. Retrieved 2019-10-28, from <http://doi.wiley.com/10.1029/2011JD017187> doi: 10.1029/2011JD017187
- Stephens, G., Winker, D., Pelon, J., Trepte, C., Vane, D., Yuhas, C., ... Lebsock, M. (2017, August). CloudSat and CALIPSO within the A-Train: Ten years of actively observing the Earth system. *Bulletin of the American Meteorological Society*. Retrieved 2018-03-07, from <https://journals.ametsoc.org/doi/abs/10.1175/BAMS-D-16-0324.1> doi: 10.1175/BAMS-D-16-0324.1
- Su, H., Jiang, J. H., Neelin, J. D., Shen, T. J., Zhai, C., Yue, Q., ... Yung, Y. L. (2017, June). Tightening of tropical ascent and high clouds key to precipitation change in a warmer climate. *Nature Communications*, 8, 15771. Retrieved 2019-01-24, from <https://www.nature.com/articles/ncomms15771> doi: 10.1038/ncomms15771
- Thompson, D. W. J., Bony, S., & Li, Y. (2017, August). Thermodynamic constraint on the depth of the global tropospheric circulation. *Proceedings of the National Academy of Sciences*, 114(31), 8181–8186. Retrieved 2018-02-11, from <http://www.pnas.org/content/114/31/8181> doi: 10.1073/pnas.1620493114
- Tompkins, A. M., & Craig, G. C. (1999, February). Sensitivity of Tropical Convection to Sea Surface Temperature in the Absence of Large-Scale Flow. *Journal of Climate*, 12(2), 462–476. Retrieved 2018-02-23, from [https://journals.ametsoc.org/doi/full/10.1175/1520-0442\(1999\)012%3C0462:SOTCTS%3E2.0.CO%3B2](https://journals.ametsoc.org/doi/full/10.1175/1520-0442(1999)012%3C0462:SOTCTS%3E2.0.CO%3B2) doi: 10.1175/1520-0442(1999)012(0462:SOTCTS)2.0.CO;2
- Wang, P.-H., McCormick, M. P., Poole, L. R., Chu, W. P., Yue, G. K., Kent, G. S., & Skeens, K. M. (1994, June). Tropical high cloud characteristics derived from SAGE II extinction measurements. *Atmospheric Research*, 34(1), 53–83. Retrieved 2020-05-13, from <http://www.sciencedirect.com/science/article/pii/0169809594900817> doi: 10.1016/0169-8095(94)90081-7
- Winker. (2018). CALIPSO Lidar Level 3 Cloud Occurrence Data, Standard V1-00 [Data set]. *NASA Langley Atmospheric Science Data Center DAAC*. doi: 10

- 495 .5067/CALIOP/CALIPSO/L3.CLOUD_OCCURRENCE-STANDARD-V1-00
 496 Winker, Chepfer, H., Noel, V., & Cai, X. (2017, November). Observational
 497 Constraints on Cloud Feedbacks: The Role of Active Satellite Sensors.
 498 *Surveys in Geophysics*, 38(6), 1483–1508. Retrieved 2018-03-09, from
 499 <https://link.springer.com/article/10.1007/s10712-017-9452-0> doi:
 500 10.1007/s10712-017-9452-0
- 501 Winker, Hunt, W. H., & McGill, M. J. (2007, October). Initial performance as-
 502 sessment of CALIOP. *Geophysical Research Letters*, 34(19), L19803. Re-
 503 trieved 2018-03-07, from [http://onlinelibrary.wiley.com/doi/10.1029/
 504 2007GL030135/abstract](http://onlinelibrary.wiley.com/doi/10.1029/2007GL030135/abstract) doi: 10.1029/2007GL030135
- 505 Xu, K.-M., Wong, T., Wielicki, B. A., Parker, L., & Eitzen, Z. A. (2005, July).
 506 Statistical Analyses of Satellite Cloud Object Data from CERES. Part
 507 I: Methodology and Preliminary Results of the 1998 El Niño/2000 La
 508 Niña. *Journal of Climate*, 18(13), 2497–2514. Retrieved 2019-07-25, from
 509 <https://journals.ametsoc.org/doi/full/10.1175/JCLI3418.1> doi:
 510 10.1175/JCLI3418.1
- 511 Xu, K.-M., Wong, T., Wielicki, B. A., Parker, L., Lin, B., Eitzen, Z. A., & Bran-
 512 son, M. (2007, March). Statistical Analyses of Satellite Cloud Object Data
 513 from CERES. Part II: Tropical Convective Cloud Objects during 1998 El
 514 Niño and Evidence for Supporting the Fixed Anvil Temperature Hypoth-
 515 esis. *Journal of Climate*, 20(5), 819–842. Retrieved 2019-07-25, from
 516 <https://journals.ametsoc.org/doi/full/10.1175/JCLI4069.1> doi:
 517 10.1175/JCLI4069.1
- 518 Yuan, J., Houze, R. A., & Heymsfield, A. J. (2011, March). Vertical Structures of
 519 Anvil Clouds of Tropical Mesoscale Convective Systems Observed by CloudSat.
 520 *Journal of the Atmospheric Sciences*, 68(8), 1653–1674. Retrieved 2019-12-04,
 521 from <https://journals.ametsoc.org/doi/full/10.1175/2011JAS3687.1>
 522 doi: 10.1175/2011JAS3687.1
- 523 Zelinka, M. D., & Hartmann, D. L. (2010, August). Why is longwave cloud feedback
 524 positive? *Journal of Geophysical Research: Atmospheres*, 115(D16), D16117.
 525 Retrieved 2017-11-10, from [http://onlinelibrary.wiley.com/doi/10.1029/
 526 2010JD013817/abstract](http://onlinelibrary.wiley.com/doi/10.1029/2010JD013817/abstract) doi: 10.1029/2010JD013817
- 527 Zelinka, M. D., & Hartmann, D. L. (2011, December). The observed sensitivity of
 528 high clouds to mean surface temperature anomalies in the tropics. *Journal of
 529 Geophysical Research: Atmospheres*, 116(D23), D23103. Retrieved 2017-11-
 530 05, from [http://onlinelibrary.wiley.com/doi/10.1029/2011JD016459/
 531 abstract](http://onlinelibrary.wiley.com/doi/10.1029/2011JD016459/abstract) doi: 10.1029/2011JD016459